Progress In Electromagnetics Research M, Vol. 42, 109–119, 2015

Effects of Inflated Cone on Satellite Radar Cross Sections in S-Band via FDTD Simulations

Shen Shou Max Chung*

Abstract—Satellites are the most important link in today's battlefield, and with the advancement of anti-satellite technologies such as anti-satellite missiles and directed energy weapons, satellites are becoming vulnerable to attack. The vulnerability of a satellite depends greatly on the probability of it being detected and tracked, and optics and radars are the two main means of detection. To avoid detection, several suggestions have been made in the past to deflect ambient light and decrease the RCS (radar cross section). The most notable RF stealth suggestion among them is the proposal of using an inflatable polymer cone to change its shape and reduce the satellite's RCS. In this study we examine the accuracy of a commercial FDTD code with a theoretical Mie scattering RCS, and use it to calculate the RCS of this so-called stealth satellite in the S-band, and analyze its frequency and radar incident angle dependence. Results indicate that this shape is advantageous in boresight monostatic backscatter RCS reduction, but in other directions the RCS increases due to the sheer size effect, which makes it even more vulnerable to bi-static radar tracking. When it is slant illuminated, the RCS of the stealth satellite shows no RCS reduction effects. This inflated device is susceptible to space debris damage and cumbersome to operate, and may interfere with the original mission of the satellite. The best strategy for satellite self-defense is orbit change.

1. INTRODUCTION

As evidenced in the two Gulf wars, information has become the decisive factor in determining the outcome of a war. C4ISR (Command, Control, Communications, Computers, Intelligence, Surveillance and Reconnaissance) capabilities have become the first priority in modern military procurements in many countries, and among the complicated links, satellites play an important role, as without satellites, transcontinental communication and over-the-horizon command are impossible.

Currently there are about 2465 satellites in orbit [1], including many already dysfunctional ones, performing military, astronomical, communication, navigational, earth observation, weather and other missions. Most of them are in LEO (Low Earth Orbit, 0–2000 km). The majority are at a distance around 500 km, and the GPS (Global Positioning Satellites) are in an SSO (Semi-synchronous Orbit) 20,350 km away, which means they orbit the earth in exactly 12 hours (twice per day). The famous International Space Station is at 340 km, and the Hubble Space Telescope at 595 km. The satellites in Sun-synchronous Orbit (600–800 km) cross the equator multiple times per day and usually at a high inclination angle relative to the equator in order to cover most of the earth's surface. Most surveillance and reconnaissance satellites use this orbit. GEO (Geosynchronous) and GSO (Geostationary) satellites orbit the earth at the same rate as the earth rotates at 35,786 km away, and they remain in a fixed location (same longitude) as observed from the earth's surface.

Satellites come in vastly different shapes, sizes and weights; most are about 500 kg in weight, and around 1 meter in diameter due to launch rocket diameter limitations. Solar panels of tens of m^2 are

Received 31 March 2015, Accepted 25 May 2015, Scheduled 3 June 2015
* Corresponding author: Shen Shou Max Chung (maxchung@ms3.hinet.net).
The author is with Center for Space and Remote Sensing Research, National Central University, Jhongli 320, Taiwan.

common sources of electrical power. Recently there has been a trend for micro-satellites (tens of kg), which are much smaller in size but tend to be limited in function and lifetime, and they travel in LEO. The kinds of satellites most likely to be attacked are military or intelligence ones, such as the KH (Keyhole) series of optical reconnaissance satellites operated by the National Reconnaissance Office [2], or those operated by the Defense Support Program [3], or similar satellites from other nations. The operational principle of these satellites can be divided into two categories: optical detection or SAR (Synthetic Aperture Radar) reconnaissance. The fundamental physics of these two categories is very similar: The lens size divided by the wavelength decides the optical resolution, and the antenna is equivalent to the lens in radar. Therefore, in order to maximize the resolution, these satellites tend to be quite big, and the telescope or antenna forms a strong source of RCS [4] back reflection. The RCS of satellites can be measured in an indoor anechoic chamber or outdoor range such as those operated by The Howland Company [5] or RATSCAT [6].

Recently several countries have demonstrated anti-satellite capability via surface-launched or air-launched anti-satellite missiles, and demonstrations of directed energy weapons have drawn connections with temporary malfunction incidents concerning several satellites. Attacking satellites is a considerable challenge, as they usually travel fairly fast ($\sim 7.5\,\mathrm{km/s}$ for RADARSAT-2), the window of attack is only a few minutes, and the altitude is about reaching the effective limit of current suitable missiles ($\sim 1000\,\mathrm{km}$ for short range ballistic missile). The missile has to travel very fast, and direct impact is preferred over detonation of the war head in the proximity. The survivability of a satellite is closely related to its detectability.

Most satellites' orbits are known from public information after the launch date, and those unannounced can be detected via optics or radars by the United States Space Surveillance Network [7]. An optical telescope can detect a satellite from the earth's surface if it reflects sun or stellar light, but cannot track them in real time. Ground-based satellite tracking radars are used and operate in the VHF band via a bi-static mechanism, such as the Air Force Space Surveillance System [8], but the new Space Fence System operates in the S-band [9]. Missiles rely on ground-based radars to provide initial mission coordinates, and the missiles themselves use on-board active radar and FPA (Focal Plane Array) to complete the final targeting. Advanced missiles usually have two on-board radars, one in the X-band to detect targets at a longer range, and one in the Ku-band to track a target in its final approach. FPA is used to distinguish decoys from targets via pattern recognition. So, even if the orbit of a satellite is known, the ability to avoid tracking by missile radars is still vital to its survival in times of emergency.

Until now, RF stealth [10] has not been an important issue in satellite design. Although today we are in an age of stealth fighters, the ordinary techniques of RF stealth are not applicable to satellites. RF stealth in airplanes is accomplished by shaping ($\sim 70\%$ effects) [10] and RAM (Radar Absorption Material, $\sim 20\%$) [11, 12], and meticulous attention to every surface detail is required. Shape design is possible in airplanes despite the fact that performances in aerodynamics may have to be sacrificed sometimes, but changes in shape are not so conveniently achieved in satellites because of the solar panels and antennas. There are several types of RAM; ferrite ones tend to be very heavy, while others may not withstand the extreme temperature changes that satellites experience during exposure to the sun and darkness. The weight increases brought by the RAM or RAS (Radar Absorption Structure) are unacceptable.

However, over the years, several interesting proposals have been made to decrease the RCS of satellites to avoid detection by radar. Barker [13] described an apparatus to camouflage portholes on satellites. Manning and Maus [14] described an interference-type radar attenuator that is composed of multiple plastic spacers compressed into a package and they can self-erect once in space to form a radar attenuator, as well as a thermal shield and meteoroid bumper. Lehman and Manning [15] described a bathtub kind of external housing for a space vehicle, with one side of the smooth surface coated with radar attenuating material and an open side for satellite functions. The shape resembles a cylinder with a quarter of a sphere at each end. Barker and Slager [16] described a crossed skirt antiradar screen structure for a space vehicle, which partially encloses the vehicle with a conducting screen, and provides an oblique angle to preclude retro-reflection of an illuminating radar beam from a ground-based radar system.

The most interesting and widely publicized idea for a stealth satellite is that of Eldridge et al. [17], in which they described an inflatable conical shield made from a thin synthetic polymer film coated

with radar reflecting material, such as gold or aluminum. A sublimation agent inflates the shield under heat, and a UV curable slurry inner coating cures the shield with the enclosed UV source. Additional means such as a boom are provided to move the shield's position with respect to the satellite. The idea of the cone shield is very simple: It is well known that a cone reflects radar signals in directions away from the boresight direction, so in facing a potential threat, the satellite must orientate itself so that the cone points in the direction of the main threat to avoid radar tracking. However, it is obvious that when the shield is in position, the functionality of the satellite is severely hindered. The original patent document states that the RCS of this design in the VHF band is decreased, and claims it reduces optical cross sections as well.

In this paper, we examine the accuracy of RCS calculation from a commercial FDTD (Finite-Difference-Time-Domain) code [18, 19], then the effectiveness of Eldridge et al.'s stealth satellite design in the S-band. First, we briefly introduce the methods available in RCS simulations, and discuss the accuracy of the code we use. Then digital models of generic and stealth satellites are described. Next we simulate the RCS of generic and stealth satellites, and finally we draw conclusions.

2. ACCURACY OF RCS MEASUREMENTS AND SIMULATION CODES

Over the years the measurement and simulation of RCS has been an extensively studied field [4, 10, 20, 21, 28], and many new anechoic chambers have been built, and there has also been progress in simulation codes [22]. Due to the high cost associated with the real measurement and accessibility of test facilities, numerical simulations are very important in terms of pre-scale-model study, trend identification and numerical experimentation. The challenges in relation to actual outdoor measurement include isolation of nearby radiation sources, multipath ground clutters, reflection from supporting structures and instrument dynamic ranges. For indoor compact range RCS measurement, the obvious limitation is the size of the quiet zone. Today, instrument errors below 0.1 dB, orientation inaccuracies of 0.5° and sensitivity of around −90 dBsm are possible in some bands. For reduced scale model RCS measurement in compact ranges, the relations between measured and real parameters are listed in Table 1. From this table one can imagine the difficulties in making a reasonable scale model with the proper materials that can truly reflect RF stealth requirements. It is almost impossible to make a RAM with reduced conductivity as specified and still retain the same ε and μ, but in simulation, it is possible.

Table 1. The relations between scale factor S and real parameters in a compact range.

Parameter	Full Scale	Subscale	Challenge
Length	L	$L' = L/S$	Easy
Wavelength	λ	$\lambda' = \lambda/S$	Difficult
Frequency	f	$f' = Sf$	Frequency into mmW range
Time	t	$t' = t/S$	Need high time resolution
Permittivity	ε	$\varepsilon' = \varepsilon$	No challenge
Permeability	μ	$\mu' = \mu$	No challenge
Conductivity	g	$g' = Sg$	Difficult to control in RAM
RCS	σ	$\sigma' = \sigma/S^2$	Error magnified

RCS simulation codes include FDTD, MOM (Method of Moment), PO (Physical Optics), etc. [22–24]. In this paper we use a commercial FDTD code. Generally speaking, FDTD can provide more accurate results providing a sufficient mesh is used, but the disadvantage is obviously the memory and time required. MOM and its derivatives can be faster, but when the object size is close to the wavelength the result errors tend to be bigger. In order to establish faith in this commercial FDTD code for the readers, we ran some example simulations and compared these with theoretical results. The most commonly used example for this purpose is the RCS of a metal sphere against theoretical

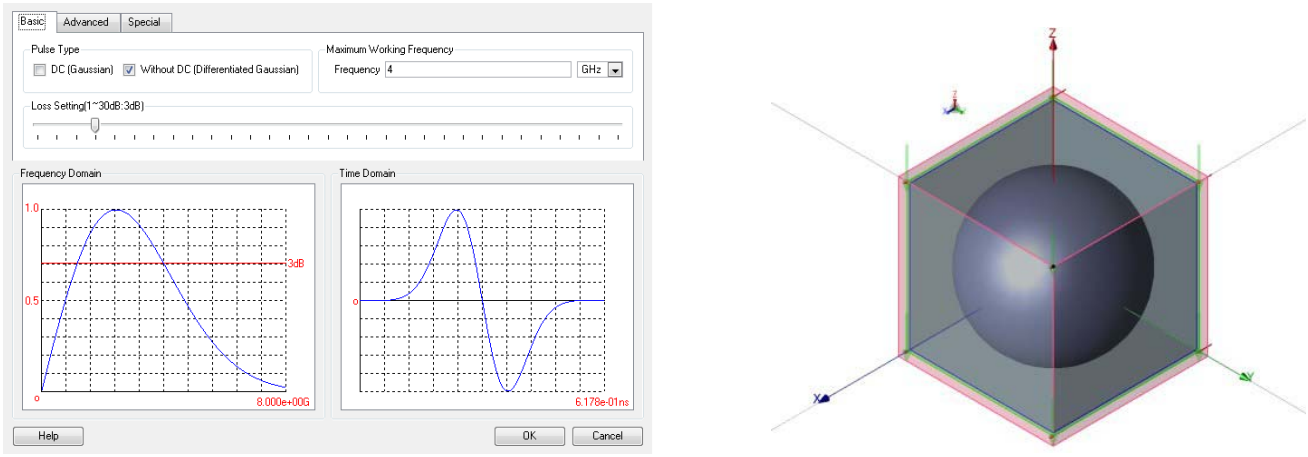

(a) (b) (c)

Figure 1. (a) The frequency and (b) time domain waveform of the incident radar signal used in this simulation. The signal is a differentiated Gaussian with a 3 dB limit between 1.5 and 5 GHz. (c) The 50 mm radius metal sphere model used to calibrate GEMS RCS results. The gray box is the Huygens box, which is the simulation volume. The green arrow indicates the radar signal incoming direction, and the red arrow shows the signal electric field polarization (X axis).

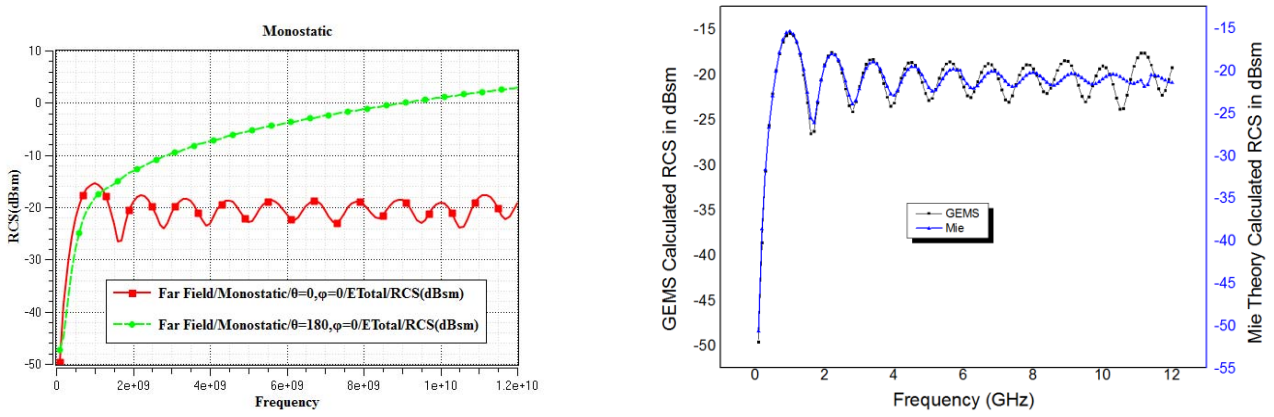

(a) (b)

Figure 2. (a) The front (red) and back (green) monostatic RCS of a 50 mm radius metal sphere between 0 and 12 GHz simulated with GEMS. (b) Comparison between RCS computed from Mie scattering theory (blue) and GEMS simulation (black) between 0 and 12 GHz.

Mie scattering RCS [25]. Figure 1(a) shows the waveform used in this simulation, while Figure 1(b) presents a 50 mm radius metal sphere model and simulation space. Figure 2(a) shows the FDTD results of the front and back RCS, and Figure 2(b) presents the results of the FDTD code overlapped with the Mie scattering results. We can see that up to 5 GHz these two results show credible consistency. The "differences" above 5 GHz may be to do with the fact that we are using a waveform that contains a range of frequencies instead of a singular one.

There are also several simple shapes with a theoretical RCS [26, 27], and we use the GEMS code to simulate a dihedral model, and the results are listed in online supplementary materials. Interested readers can make a dihedral model and measure it in your anechoic room, but bear in mind that theoretical results are not always as "real" as they appeared in radar due to complicated system configurations and the waveforms you use.

3. DIGITAL MODELS OF GENERIC AND STEALTH SATELLITES

Although satellites come in many shapes and sizes, in terms of RCS, the most important thing is the dominant scattering source, and the so-called RCS numbers game [28]. Put simply, a larger size or complicated surface morphology does not necessarily constitute a strong scattering source, and reducing the scattering from a secondary scattering source does not diminish the whole RCS very much; the most important work in RCS reduction is to diminish the contribution from the dominant scattering source.

For this reason, we choose a simple cylinder shape as our generic satellite model with the solar cell representing the dominant scattering source. This structure is similar to the one outlined in the original patent literature of Eldridge et al. [17], and we build it roughly to the size of the famous Lacrosse/Onyx satellites [29], which when shielded by the inflated polymer cone is the rumored "Misty Satellite" on the Internet. Due to the large size of this satellite, it is quite hard to really achieve RF stealth in the VHF or S band with traditional means. Its large size also makes it an electrically large object for RCS simulation, and considerable computation time is involved.

Depicted in Figure 3(a) is the digital model of the generic satellite. The main satellite body (yellow) is a cylinder with a radius of 2 m and 10 m long, and is covered by a Si surface representing solar cells. Below the main body are two retractable square solar cell panels (blue); each is 4×8 m wide and 0.2 m thick. The insert is a correspondence between spherical and rectangular coordinate systems. Depicted in Figure 3(b) is the stealth satellite model with the polymer cone shield extended. The cone shield is composed of a large cone and a shallow dish bottom. The radius of the cone shield at the bottom is 13 m and the cone height is 40 m. The cone angle is close to 52°. A smaller cone angle would have given a better RF stealth performance, but the size would also be considerably larger. The surface of the shield is assumed to be a thin film coated with gold to deflect electromagnetic waves. The bottom of the shield is gently curved like a dish to avoid sharp edges that may cause retro-reflections. The shield is connected to the satellite's main body with a boom that can rotate the shield 90 degrees to the parallel X axis when necessary in order to perform its original function. The radar waveform in Figure 1(a) is used, which illuminates the satellite from the Z direction, with electric field polarization in the positive X direction.

4. RCS COMPARISONS OF THE GENERIC AND STEALTH SATELLITES IN BORESIGHT ILLUMINATION

RCS is a function of frequency, polarization, viewing angle, shape, material, waveform and bandwidth. Here we draw the RCS of these two satellites at 2, 3 and 4 GHz in the S-band, a common band for long-range surveillance with a better resolution than VHF radar. We use the GEMS code to simulate the RCS. A certain waveform is assumed to illuminate on the Huygens box, which is not just a plane wave of a single frequency, but one that contains a certain bandwidth (Figure 1(a)). The reflected electric field is calculated according to the material of the object and then the RCS is calculated. The near field to far field transformation can be made using the Geometric Mean method [30] or others. The dispersion errors are not obvious until they are larger than 5 GHz (Figure 2(b)). The simulations were performed using an i7 machine with 16 GB of memory installed. Running time ranges from 20 to 50 hours depending on the grid and time steps used.

4.1. The RCS of Generic and Stealth Satellites in Boresight Illumination

Figure 4(a) is the front (red) and back (green) monostatic RCS of the generic satellite. As we can see, the front monostatic ($\theta = 0°$, $\varphi = 0°$) RCS is generally smaller than the rear-end view ($\theta = 180°$, $\varphi = 0°$), which is common in this Feature Size/$\lambda \gg 1$ scenario. The ($\theta = 180°$, $\varphi = 0°$) monostatic RCS is the radar in the ($\theta = 0°$, $\varphi = 0°$) direction and the receiver in the ($\theta = 180°$, $\varphi = 0°$) direction.

Figure 4(b) is the front (red) and back (green) monostatic RCS of the stealth satellite. We can see now that the front and back monostatic RCS values are much closer to each other; this may be caused by the huge cone, which dominates the visual area in both directions. Compared with Figure 4(a), we can see the RCS reduction effects clearly.

Figure 5(a) is the RCS of the generic satellite at $\theta = 90°$ cut (which is the X-Y plane) at 2 (red), 3 (green) and 4 (blue) GHz. We can see that the maximum RCS of the generic satellite occurs on the four

axes ($\varphi = 0°$, 90°, 180° and 270°) due to the symmetry of the structure and electric field polarization in the X direction, and is particularly large at $\varphi = 90°$ and 270°, as a result of the solar panels and their perpendicularity to the electric field polarization. At 4 GHz, there are an additional four peaks at $\varphi = 75°$, 108°, 253° and 288°, which may be the result of creeping waves. We can also see, as the frequency increases from 2 to 4 GHz, that the RCS variations in each individual direction could have changed by 10 dBsm, sometimes more. Generally speaking, RCS is smaller in 2 GHz for an obvious reason. RCS in most directions is below 0 dBsm, while the maximum on the Y axis reaches 25 dBsm,

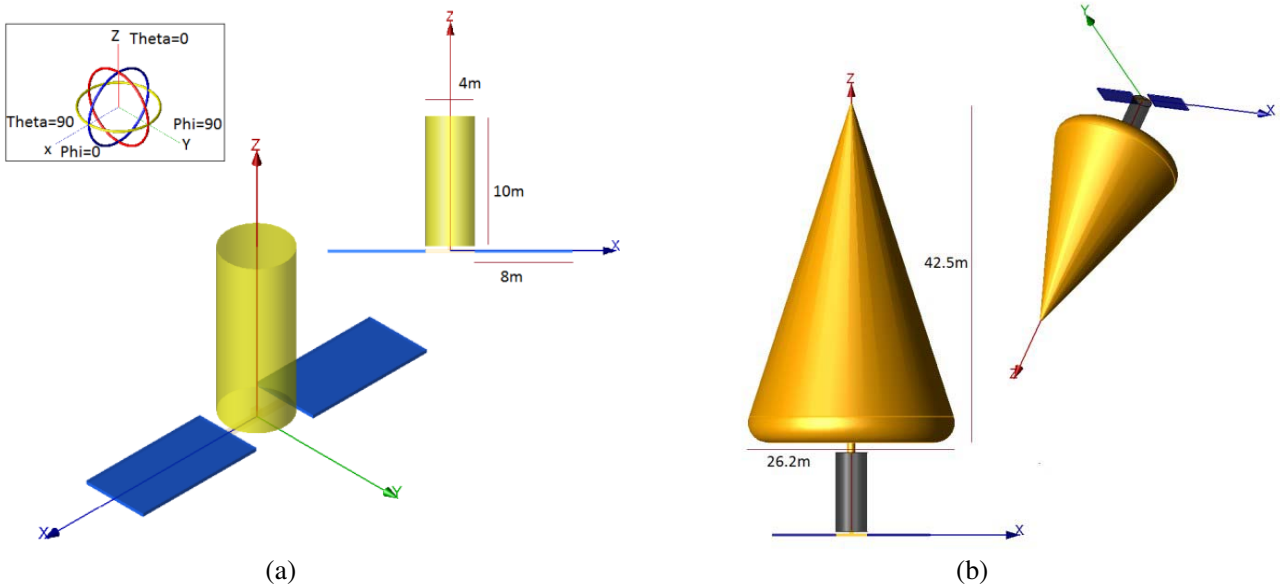

Figure 3. (a) Digital model of a generic reconnaissance satellite. The main satellite body (yellow) is a cylinder with a radius of 2 m and 10 m long, and the two retractable solar cell panels (blue) are both 4×8 m wide and 0.2 m thick. The upper left insert is a correspondence between the spherical and the rectangular coordinate system. The upper right insert is the X-Z plane view of the satellite. (b) The X-Z plane and 3D view of the digital model for a stealth satellite with an inflated cone placed in front of it. The bottom radius of the inflatable cone is 13.1 m and the cone height is 42.5 m, which forms a cone angle of roughly 52°. The surface of the cone is assumed to be coated with gold.

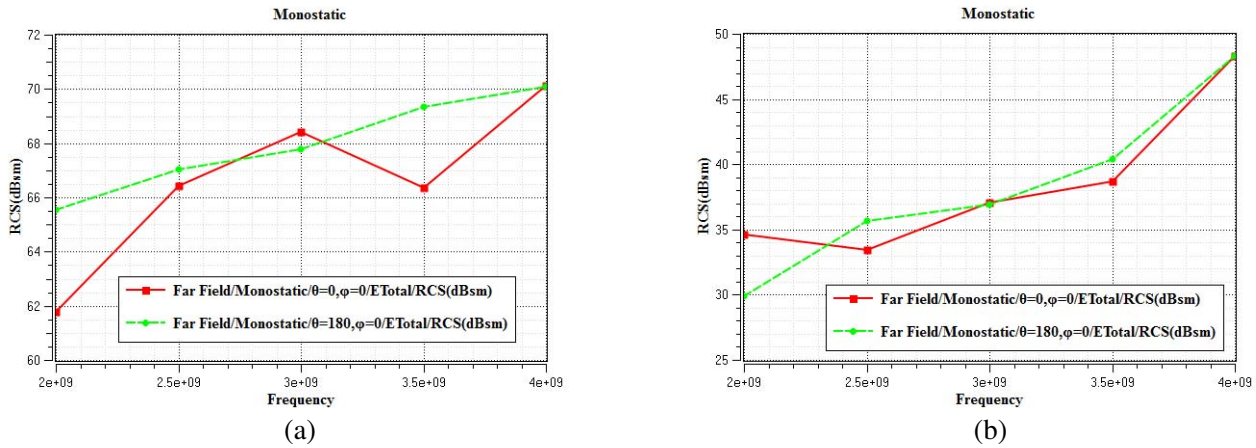

Figure 4. (a) The front (red) and back (green) monostatic RCS of the generic satellite in the S-band. (b) The front (red) and back (green) monostatic RCS of the stealth satellite in the S-band.

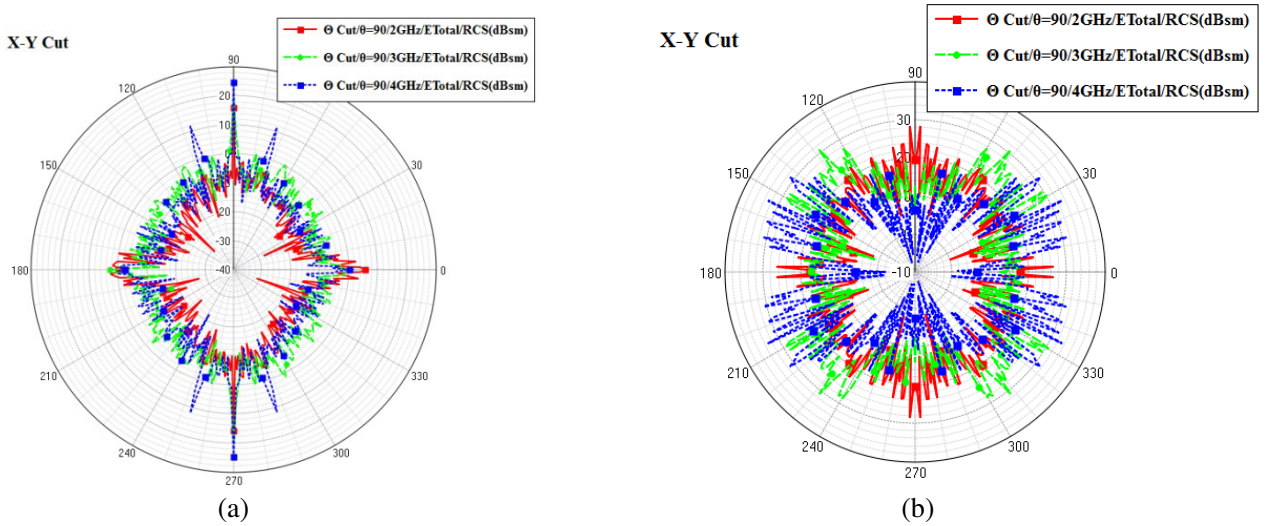

Figure 5. (a) The RCS of the generic satellite at $\theta = 90°$ (which is the X-Y plane) for 2 (red), 3 (green) and 4 (blue) GHz. (b) The RCS of the stealth satellite at the same cut.

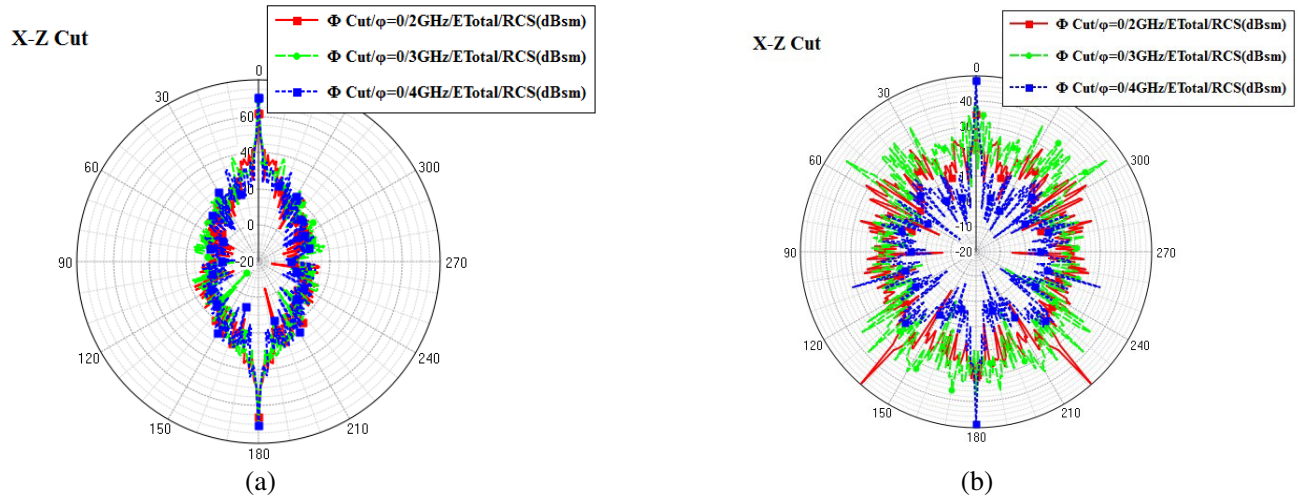

Figure 6. (a) The RCS of the generic satellite at a cut of $\varphi = 0°$ (which is the X-Z plane) for 2 (red), 3 (green) and 4 (blue) GHz. (b) The RCS of the stealth satellite at the same cut.

which is equivalent to a small ship (actually, the size of this satellite is equivalent to a small ship).

Figure 5(b) is the RCS of the stealth satellite at the same cut. We can see that the RCS on the stealth satellite is actually larger than that on the generic satellite in many directions, mainly because the stealth satellite is much larger than the generic satellite in the X-Y plane. The RCS maximums are between 20 and 35 dBsm with peaks rotating with frequencies due to creeping waves. The differences between 2, 3 and 4 GHz are also amplified because of the creeping waves.

Figure 6(a) is the RCS of the generic satellite at a cut of $\varphi = 0°$ (which is the X-Z plane) at 2 (red), 3 (green) and 4 (blue) GHz. We can see that the RCS pattern is very different from Figure 5(a), with the largest RCS directions at $\theta = 0°$ and $180°$ (Z axis), and values reaching 60 dBsm. This is a simple effect of the two perpendicular angles formed by the solar panel and the main body, together with the front face of the solid cylinder. The smallest RCS occurs at $\theta = 90°$ and $270°$ (X axis) with values around ± 10 dBsm, as the solar panel is almost invisible in this view direction.

Figure 6(b) is the RCS of the stealth satellite at a cut of $\varphi = 0°$. Compared with Figure 6(a), the RCS maximums no longer appear on the Z axis, as now for 2 GHz they appear at $\theta = 140°$ and $220°$,

reaching the 50 dBsm level, while the boresight RCS has decreased from the generic satellite's 65 dBsm to $\sim$ 35 dBsm at 2 GHz, 70 dBsm to 40 dBsm at 3 GHz, and 70 dBsm to 48 dBsm at 4 GHz. This is the main RCS reduction effect of the polymer cone. So in principle, if the radar is illuminating from the boresight direction, the cone shield concept works.

Figure 7(a) is the RCS of the generic satellite at a cut of $\varphi = 90°$ (which is the Y-Z plane) at 2 (red), 3 (green) and 4 (blue) GHz. Compared with Figure 6(a), the RCS pattern is different because we are now observing from another symmetry angle of the solar panels. We can see two maximums at $\theta = 0°$ and 180° as in Figure 6(a), with values between 60 and 70 dBsm. The RCS at most angles is larger than in Figure 6(a). The minimums appear at different angles as the frequencies vary.

Figure 7(b) is the RCS of the stealth satellite at the same cut as in Figure 7(a). We can see that at 2 GHz, the boresight RCS on the Z axis is about 35 dBsm now, a much smaller value than the 65 dBsm of the generic satellite. At 3 and 4 GHz the comparison becomes 40 dBsm (stealth) to 70 dBsm (generic) and 48 dBsm (stealth) to 70 dBsm (generic). In other directions, the RCS is a bit smaller than the generic satellite (please note that the RCS scale in Figures 7(a) and 7(b) is different), and the distribution is vastly different.

Figure 8(a) is the 3D RCS of the generic satellite at 3 GHz drawn at a resolution of 10°, and the

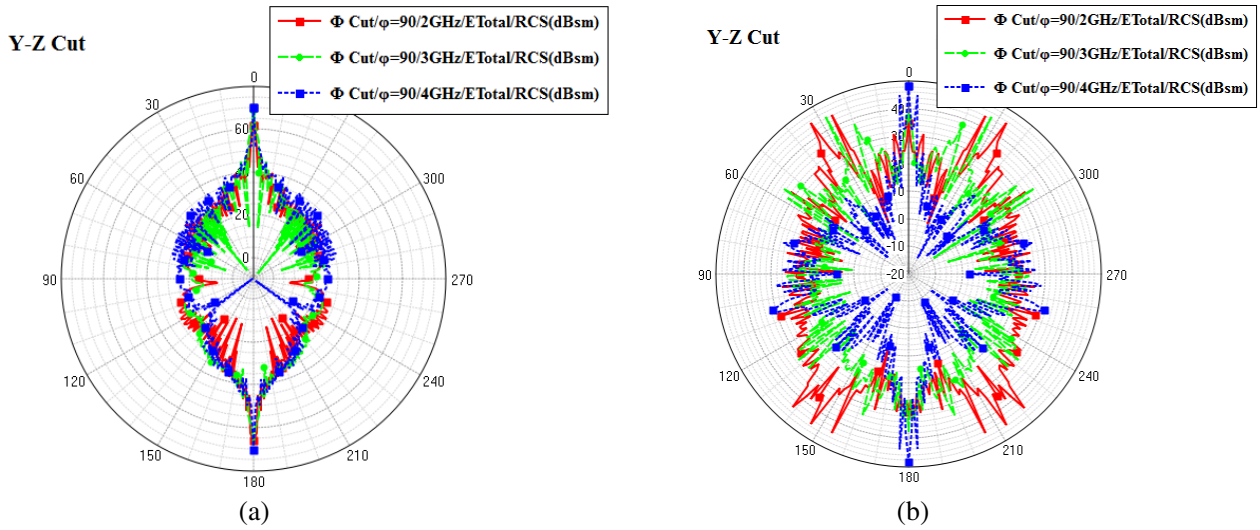

(a) (b)

Figure 7. (a) The RCS of the generic satellite at $\varphi = 90°$ (which is the Y-Z plane) for 2 (red), 3 (green) and 4 (blue) GHz. (b) The RCS of the stealth satellite at the same cut.

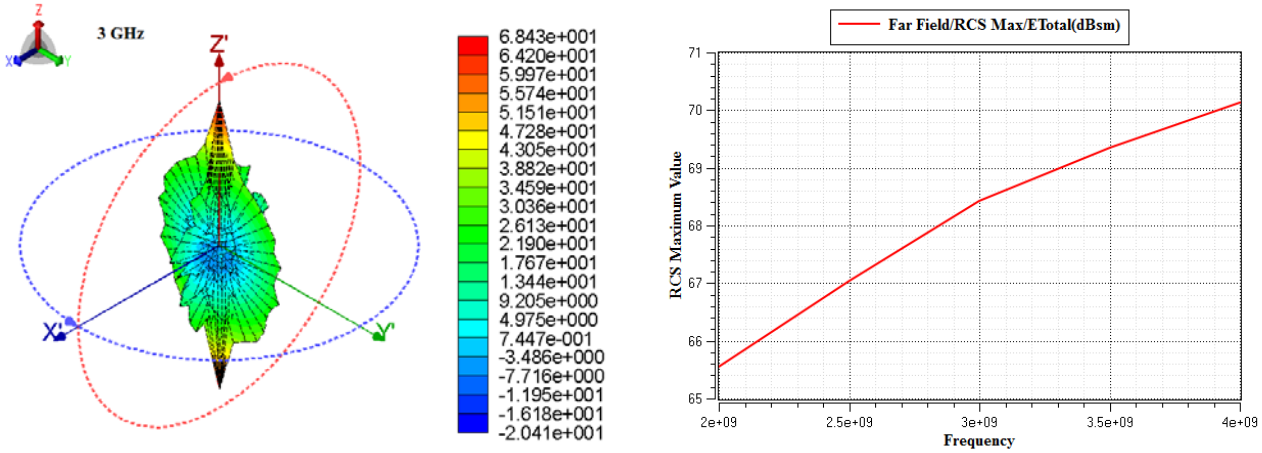

(a)

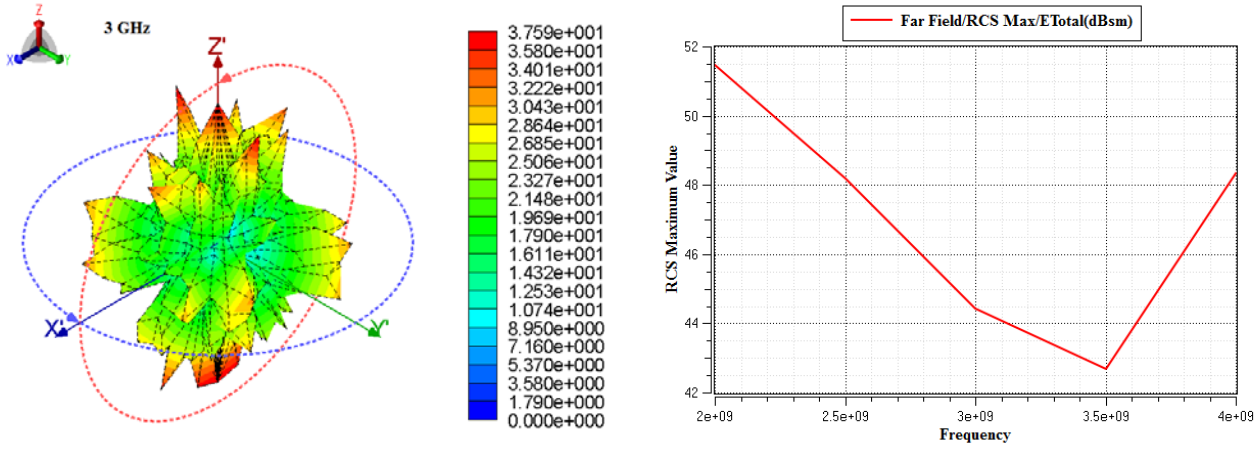

(b)

Figure 8. (a) The 3D RCS of the generic satellite at 3 GHz at a resolution of 10°, and the maximum value of RCS at various frequencies. (b) The 3D RCS of the stealth satellite at 2, 3 and 4 GHz at a resolution of 10°, and the maximum value of RCS at various frequencies.

maximum RCS values at various frequencies. The 3D views provide a global feeling of what the RCS may look like, but the impression can be quite different if drawn at a finer resolution. As stated, the maximum values appear on the Z axis for this shape, and this value increases as the frequency increases.

Figure 8(b) is the 3D RCS of the stealth satellite at 3 GHz at a resolution of 10°, and the maximum RCS values at various frequencies. Compared with Figure 9(a), many peaks appear. The maximum of the RCS chart shows the RCS reduction effect of the polymer cone very well, and compared with Figure 8(a), the maximum values in many frequencies drop considerably. However, since we cannot be sure the maximum always occurs in the boresight direction, Figures 4(a) and 4(b) make a direct comparison of monostatic RCS at the boresight.

4.2. The RCS of Generic and Stealth Satellites under Slant Illumination

We have also simulated the RCS of these two satellite models under 45° (relative to the Z axis on the X-Y plane) illumination, and the results are listed as online supplementary materials due to page limitation. The results indicate that there is no obvious RCS reduction effect under slant illumination. The front monostatic RCS of the generic satellite is 24, 28 and 13 dBsm at 2, 3 and 4 GHz, while the stealth satellite is 23, 27 and 36 dBsm. The front monostatic RCS of the generic satellite is larger than the back monostatic RCS when the frequency is less than 3 GHz, while for the stealth satellite, the front monostatic RCS is smaller than the back monostatic RCS when the frequency is less than 3.5 GHz. The 3D RCS figure also shows quite distinctive features between these two models.

5. CONCLUSIONS

From previous analysis of the RCS between these two digital models, we can see a significant RCS reduction when it is shined on by S-band radar in the boresight direction. However, significant RCS increases are also observed in the perpendicular direction (X-Y plane), so this actually increases the possibility of detection by bi-static ground-based radar, as it usually shines on the side of the satellite when the satellite's antenna or telescope is directed towards the earth's surface. As stated previously, nowadays it is difficult for satellites to hide from ground-based bi-static radars [9], so mission planners can prescribe a missile trajectory to intercept most satellites. When the missile approaches the target satellite, the stealth satellite either has to raise its cone pointing towards the missile to camouflage itself from the X- and Ku-band target-seeking radars on the missile to avoid tracking, or has to point this

cone towards the ground-based radar to discontinue uplinking coordinate information. The effect of this shield in the X- and Ku-band is beyond the capability of our present computing facility.

In reality, one disadvantage of this cone design is the integrity of its structure. Because it is quite large and thin, it makes it quite vulnerable to space debris damage. High-speed debris can easily penetrate the polymer shield and deflate the gas inside, consequently causing the structure to collapse. Another disadvantage is that the shield itself seriously interferes with the main function of the satellite, which is to reconnoiter surface objects. Moving the shield 90° sideways with a boom may take considerable precious time to complete.

In conclusion, the best defense of satellites against missile attack is still trying to design with a stealth shape from the beginning, both in RF and in optics. Inevitably all satellites will be spotted because of their fixed orbit, but in times of emergency, changing orbit or outrunning the missile while releasing chaff may be a good escape strategy. However, changing orbits can only be accomplished a few times within the lifetime of the satellite due to limited fuel capacity, so extra fuel is needed in the design stage. There are also other options for providing RF stealth capability to satellites, such as plasma stealth [31], and how to apply this technique in satellites will be discussed on another occasion.

ACKNOWLEDGMENT

The authors would like to thank the CSRSR (Center for Space and Remote Sensing Research) of National Central University for hosting this project, and Computer and Communication Unlimited together with the Dorchia Communications Company, Taiwan, for providing a provisional license and technical assistance for the GEMS simulation software. We are also grateful to the National Center for High-performance Computing (NCHC) for providing computer time and facilities. This project is sponsored by the National Science Council (NSC) of Taiwan under project NSC 101-2811-M-008-087.

REFERENCES

1. Satellites, http://en.wikipedia.org/wiki/Satellite.
2. National Reconnaissance Office, http://en.wikipedia.org/wiki/National_Reconnaissance_Office.
3. Defense Support Program, http://en.wikipedia.org/wiki/Defense_Support_Program.
4. Knott, E. F., *Radar Cross Section Measurement*, Van Norstrand Reinhold, New York, 1993.
5. The Howland Company, http://www.thehowlandcompany.com/index.htm.
6. RATSCAT, http://virtualglobetrotting.com/map/radar-target-scatter-ratscat-range/.
7. United States Space Surveillance Network, http://en.wikipedia.org/wiki/United_States_Space_Surveillance_Network.
8. Air Force Space Surveillance System, http://en.wikipedia.org/wiki/Air_Force_Space_Surveillance_System.
9. Space Fence, http://www.lockheedmartin.com/us/products/space-fence.html.
10. Lynch, Jr., D., *Introduction to RF Stealth*, SciTech Publishing Inc., Raleigh, NC, 2004.
11. Vinoy, K. J. and R. M. Jha, *Radar Absorbing Materials: From Theory to Design and Characterization*, Kluwer Academic Publishers, Boston, MA, 1996.
12. Saville, P., "Review of radar absorbing materials," Technical Memorandum, DRDC Atlantic, 2005, available on line at http://www.dtic.mil/dtic/tr/fulltext/u2/a436262.pdf.
13. Barker, W. C., *Radar Camouflage Arrangement*, US Patent 3,233,238, Feb. 1, 1966.
14. Manning, W. P. and L. Maus, *Self Erectable Structure*, US Patent 4,044,358, Aug. 23, 1977.
15. Lehman, T. H. and W. P. Manning, *Vehicle Shield*, US Patent 4,947,174, Aug. 7, 1990.
16. Barker, W. C. and D. M. Slager, *Cross Skirt Antiradar Screen Structure for Space Vehicle*, US Patent 6,107,952, Aug. 22, 2000.
17. Eldridge, M. T., K. H. McKechnie, and R. M. Hefley, *Satellite Signature Suppression Shield*, US Patent 5,345,238, Sep. 6, 1994.

18. Mittra, R. and W. Yu, "General-purpose EM solver (GEMS): A new simulation tool for modeling large-scale electromagnetic systems on parallel platforms," *Joint Seminar of the IEEE Ottawa AP/MTT*, CPMT, EMC Chapters and Department of Electronics, Carleton University, May 5, 2009, available online at http://www.ottawa.ieee.ca/ap_mtt/docs/Mittra_Yu_may_51.pdf.
19. GEMS: http://www.2comu.com/.
20. Skolnik, M., *Radar Handbook*, 3rd Edition, McGraw-Hill Professional, 2008.
21. Ufimtsev, P. Ya., *Fundamentals of the Physical Theory of Diffraction*, 1st Edition, Wiley-IEEE Press, Feb. 16, 2007.
22. FEKO, https://www.feko.info/, CST, https://www.cst.com/, EMPIRE, http://www.empire.de/, HFSS, http://www.ansys.com, XFDTD, http://www.remcom.com/xf7, Efields: http://www.efieldsolutions.com/, EMPRO, http://www.home.agilent.com, cadRCS: http://www.cadrcs.com/en/start.html, CAST, http://virtual.vtt.fi/virtual/proj2/cast/, NEC2, http://www.nec2.org/.
23. Uluisik, Ç., M. Çakir, and L. Sevgi, "Radar cross section (RCS) modeling and simulation, Part 1: A tutorial review of definitions, strategies, and canonical examples," *IEEE Ant. and Prop. Mag.*, Vol. 50, No. 1, 115–126, Feb. 2008.
24. Çakir, G., M. Çakir, and L. Sevgi, "Radar cross section (RCS) modeling and simulation, Part 2: A novel FDTD-based RCS prediction virtual tool for the resonance regime," *IEEE Ant. and Prop. Mag.*, Vol. 50, No. 2, 81–94, Apr. 2008.
25. Mie Scattering Theory, http://www.mathworks.com/matlabcentral/fileexchange/36062-calculation-of-radar-cross-section-rcs-using-mie-theory.
26. Crispin, Jr., J. W. and A. L. Maffett, "Radar cross-section estimation for simple shapes," *Proceedings of the IEEE*, Vol. 53, No. 8, 833–848, Aug. 1965.
27. RCS Benchmark for Simple Shapes: http://www.emcos.com/wp-content/uploads/2014/03/Application_Note_RCS_Benchmark_Simple_Shapes.pdf.
28. Knott, E. F., J. F. Schaeffer, and M. T. Tuley, *Radar Cross Section*, 274, SciTech Publishing Inc., 2004.
29. Lacrosse (satellite), http://en.wikipedia.org/wiki/Lacrosse_(satellite).
30. *Understanding the FDTD Method, Chapter 14, Near-To-Far-Field Transformation*, http://www.eecs.wsu.edu/_schneidj/ufdtd/chap14.pdf.
31. Chung, S. S. M., "FDTD simulations on radar cross sections of metal cone and plasma covered metal cone," *Vacuum*, Vol. 86, No. 7, 970–984, Feb. 8, 2012.